

Monte Carlo simulation of nonlinear Couette flow in a dilute gas

José María Montanero^{a)}

Departamento de Electrónica e Ingeniería Electromecánica,
Universidad de Extremadura, E-06071 Badajoz, Spain

Andrés Santos^{b)} and Vicente Garzó^{c)}

Departamento de Física, Universidad de Extremadura,
E-06071 Badajoz, Spain
(May 25, 2024)

The Direct Simulation Monte Carlo method is applied to solve the Boltzmann equation in the steady planar Couette flow for Maxwell molecules and hard spheres. Nonequilibrium boundary conditions based on the solution of the Bhatnagar-Gross-Krook (BGK) model for the Couette flow are employed to diminish the influence of finite-size effects. Non-Newtonian properties are characterized by five independent generalized transport coefficients: a viscosity function, a thermal conductivity function, two viscometric functions, and a cross coefficient measuring the heat flux orthogonal to the thermal gradient. These coefficients depend nonlinearly on the shear rate. The simulation results are compared with theoretical predictions given by the Grad method and the BGK and the ellipsoidal statistical (ES) models. It is found that the kinetic models present a good agreement with the simulation, especially in the case of the ES model, while the Grad method is only qualitatively reliable for the momentum transport. In addition, the velocity distribution function is also measured and compared with the BGK and ES distributions.

PACS numbers: 47.50.+d, 51.10.+y, 05.20.Dd, 05.60.-k

I. INTRODUCTION

One of the most interesting states for analyzing transport processes far from equilibrium is the steady planar Couette flow. The physical situation corresponds to a system enclosed between two infinite, parallel plates in relative motion and, in general, kept at different temperatures. These boundary conditions lead to combined heat and momentum transport. If x and y denote the coordinates parallel to the flow and orthogonal to the plates, respectively, then the corresponding steady hydrodynamic balance equations are

$$\frac{\partial P_{xy}}{\partial y} = \frac{\partial P_{yy}}{\partial y} = 0, \quad (1)$$

$$P_{xy} \frac{\partial u_x}{\partial y} + \frac{\partial q_y}{\partial y} = 0, \quad (2)$$

where $\mathbf{u} = u_x \hat{\mathbf{x}}$ is the flow velocity, \mathbf{P} is the pressure tensor, and $\mathbf{q} = q_x \hat{\mathbf{x}} + q_y \hat{\mathbf{y}}$ is the heat flux. The presence of q_y in Eq. (2) indicates that a thermal gradient $\partial T / \partial y$ is induced by the velocity gradient, even if both plates are kept at the same temperature. The balance equations (1) and (2) do not constitute a closed set unless the dependence of the pressure tensor and the heat flux on the hydrodynamic fields is known. If the gradients are small, the fluxes \mathbf{P} and \mathbf{q} are described by the Navier-Stokes (NS) constitutive relations, which in this problem yield

$$P_{xx} = P_{yy} = P_{zz}, \quad P_{xy} = -\eta_0 \frac{\partial u_x}{\partial y}, \quad (3)$$

$$q_x = 0, \quad q_y = -\kappa_0 \frac{\partial T}{\partial y}, \quad (4)$$

where η_0 and κ_0 are the NS shear viscosity and thermal conductivity coefficients, respectively. As a consequence of the absence of normal stress differences in the NS description, the hydrostatic pressure $p = (P_{xx} + P_{yy} + P_{zz})/3$ is a constant, on account of the balance equation (1).

Even in the linear regime described by the NS equations, one still needs to know the spatial dependence of the transport coefficients to obtain the exact solution of the hydrodynamic equations. The problem becomes tractable

in the case of a low density gas, where the state of the system is completely specified by the velocity distribution function $f(\mathbf{r}, \mathbf{v}; t)$, which obeys the Boltzmann equation.¹ The Chapman-Enskog solution² of this equation shows that the ratio η_0/κ_0 is a constant. From the NS hydrodynamic equations (1)–(4) it then follows that the flow velocity profile is quasi-linear,

$$\eta_0 \frac{\partial u_x}{\partial y} = \text{const}, \quad (5)$$

and the temperature is quasi-parabolic,

$$\left(\kappa_0 \frac{\partial}{\partial y} \right)^2 T = - \frac{\kappa_0}{\eta_0} \left(\eta_0 \frac{\partial u_x}{\partial y} \right)^2 = \text{const}. \quad (6)$$

Note that the profile of u_x is not strictly linear, due to the space dependence of η_0 through the temperature. Analogously, the temperature profile is not strictly quadratic. In fact, the specific form of both profiles depends on the interaction potential under consideration. On the other hand, from Eqs. (5) and (6) it is easy to derive a nice result, namely that if the temperature T is seen as a function of u_x rather than as a function of the coordinate space y , then one has

$$\frac{\partial^2 T}{\partial u_x^2} = - \frac{\eta_0}{\kappa_0}. \quad (7)$$

This is a sort of nonequilibrium “equation of state,” according to which the temperature is a quadratic function of the flow velocity. Moreover, the “curvature” of the profile is practically universal, given the weak influence of the interaction potential on the Prandtl number $\text{Pr} = 5k_B\eta_0/2m\kappa_0 \simeq \frac{2}{3}$, where k_B is the Boltzmann constant and m is the mass of a particle.

On the other hand, when the strength of the gradients is not small, the NS relations are not expected to hold and the transport must be described by nonlinear constitutive equations. In the special case of Maxwell molecules (particles interacting via an r^{-4} potential), it has been shown^{3,4} that the Boltzmann equation admits a consistent solution in the *nonlinear* Couette flow characterized by a constant pressure p and profiles similar to those obtained in the NS regime, Eqs. (5)–(7), except that η_0 and κ_0 are replaced by a generalized shear viscosity coefficient $\eta(a) = \eta_0 F_\eta(a)$ and a generalized thermal conductivity coefficient $\kappa_{yy}(a) = \kappa_0 F_\kappa(a)$, respectively. Here, $a = (\eta_0/p)\partial u_x/\partial y$ is a constant (dimensionless) shear rate and F_η and F_κ are nonlinear functions of a . In addition, $P_{xx} \neq P_{yy} \neq P_{zz}$ and $q_x \neq 0$. This solution describes heat and momentum transport for arbitrary velocity and thermal gradients in the bulk domain, where boundary effects are negligible. On the other hand, the full nonlinear dependence of $F_\eta(a)$ and $F_\kappa(a)$ is not explicitly known, since it involves the infinite hierarchy of moment equations. Their knowledge is limited to super-Burnett order and the result is⁴ $F_\eta(a) = 1 - 3.111a^2$ and $F_\kappa(a) = 1 - 7.259a^2$.

Consequently, if one wants to get the transport properties for arbitrary values of the shear rate and the thermal gradient, one must resort to approximate schemes or to computer simulations. In the first alternative, explicit expressions for the nonlinear transport coefficients in the Couette flow have been obtained from exact solutions of the Bhatnagar-Gross-Krook (BGK) model^{5,6} and related models^{7–9} for general interactions, as well as from the Grad method.¹⁰ In the simulation side, Risso and Cordero¹⁰ have recently studied the shear-rate dependence of F_η and F_κ by means of molecular dynamics simulations of a hard disk gas. Comparison between the different analytical results with those obtained from the simulation shows that the predictions given by kinetic models are in better agreement than those given by the Grad method, especially in the case of the thermal conductivity.⁹ Nevertheless, given the difficulties associated with molecular dynamics simulations to achieve large shear rates in a dilute gas, the above comparison is restricted to a range of shear rates for which non-Newtonian effects are hardly significant. For instance, the shear viscosity has only decreased around 10% with respect to its Navier-Stokes value for the largest value of the shear rate considered by Risso and Cordero.¹⁰ In order to overcome such difficulties and extend the range of values of a , one may use the so-called Direct Simulation Monte Carlo (DSMC) method,¹¹ which is known to qualify as an efficient and accurate method to numerically solve the Boltzmann equation.

The aim of this paper is to solve the Boltzmann equation by means of the DSMC method for a gas subjected to the planar Couette flow. The motivation of this work is twofold. On the one hand, we want to test the reliability of the far from equilibrium results obtained from kinetic models and the Grad method by making a comparison with the Boltzmann solution in the case of Maxwell molecules, for which the form of the hydrodynamic profiles in the bulk region (far from the boundaries) is known. We will determine not only the hydrodynamic profiles but also the nonlinear transport coefficients and the velocity distribution function. On the other hand, we want to investigate whether the above results for a system of Maxwell molecules extend to other interaction potentials. This extension holds when the Boltzmann equation is replaced by kinetic models where, in terms of a conveniently scaled space

variable, all the results are independent of the interaction law. Thus, we will also solve numerically the Boltzmann equation for a hard-sphere gas.

Since we are interested in describing transport properties in the bulk region, i.e., free from finite-size effects, we need to use appropriate boundary conditions in the simulations. In the conventional boundary conditions,^{10,12} the gas is assumed to be enclosed between two baths *at equilibrium* in relative motion and, in general, at different temperatures. Under these conditions, a particle leaving the system is formally replaced by a particle coming from the bath, so that the incoming velocity is sampled from a local equilibrium distribution. As a consequence, there exists a mismatch between the velocity distribution function of the reemitted particles and that of those particles of the gas located near the wall and moving along the same direction. In this case, in order to inhibit the influence of boundary effects one needs to take very large systems (normal distance between the plates much larger than the mean free path), what is not practical from a computational point of view. To overcome this difficulty, a possibility is to assume that both baths are out of equilibrium in a state close to that of the actual gas. Since such a state is not known “*a priori*”, in this paper we assume that the state of the baths is described by the BGK solution of the planar Couette flow.⁶ Although the boundary effects are still unavoidable, we expect that the above mismatch between reemitted and gas particles will be much smaller. As a matter of fact, the use of these conditions has been shown to be appropriate to analyze bulk transport properties in the special case of planar Fourier flow (both walls at rest).¹³

The plan of the paper is as follows. In Sec. II we give a brief description of the planar Couette flow and a summary of the main results obtained from the Boltzmann equation and kinetic models. The boundary conditions used in the simulations and the DSMC method are described in Sec. III. Section IV presents the main results of the paper, where special attention is paid to the nonlinear transport coefficients. A comparison with the analytical results derived from the BGK and the ellipsoidal statistical (ES) models and from the Grad method is also carried out. The comparison shows in general a good agreement of the kinetic models with computer simulations, even for large shear rates. In addition, the velocity distribution function obtained in the bulk domain from the simulation is compared with the ones given by the kinetic models. It is shown again that the agreement is qualitatively good. We close the paper in Sec. V with some concluding remarks.

II. DESCRIPTION OF THE PROBLEM AND SUMMARY OF THEORETICAL RESULTS

Let us consider a dilute gas. In this case, a kinetic description is sufficient to characterize the state of the system by means of the velocity distribution function $f(\mathbf{r}, \mathbf{v}; t)$. This distribution function obeys the nonlinear Boltzmann equation, which in the absence of external forces is given by¹

$$\frac{\partial f}{\partial t} + \mathbf{v} \cdot \nabla f = J[f, f], \quad (8)$$

where

$$J[f, f] = \int d\mathbf{v}_1 \int d\hat{\mathbf{k}} g I(g, \hat{\mathbf{k}}) [f(\mathbf{v}') f(\mathbf{v}'_1) - f(\mathbf{v}) f(\mathbf{v}_1)] \quad (9)$$

is the collision operator. In this equation, $I(g, \hat{\mathbf{k}})$ is the differential cross section, $g \equiv |\mathbf{v} - \mathbf{v}_1|$ being the relative velocity, and $(\mathbf{v}', \mathbf{v}'_1)$ are precollisional velocities yielding postcollisional velocities $(\mathbf{v}, \mathbf{v}_1)$. From the distribution function, one may define the hydrodynamic quantities

$$n = \int d\mathbf{v} f, \quad (10)$$

$$\mathbf{u} = \frac{1}{n} \int d\mathbf{v} \mathbf{v} f, \quad (11)$$

$$\frac{3}{2} n k_B T = \frac{m}{2} \int d\mathbf{v} \mathbf{V}^2 f, \quad (12)$$

and the momentum and heat fluxes

$$\mathbf{P} = m \int d\mathbf{v} \mathbf{V} \mathbf{V} f, \quad (13)$$

$$\mathbf{q} = \frac{m}{2} \int d\mathbf{v} \mathbf{V}^2 \mathbf{V} f. \quad (14)$$

Here, n is the number density, \mathbf{u} is the flow velocity, T is the temperature, \mathbf{P} is the pressure tensor, \mathbf{q} is the heat flux, and $\mathbf{V} = \mathbf{v} - \mathbf{u}$ is the peculiar velocity. In addition, the equation of state is that of an ideal gas, i.e., $p = nk_B T$.

Most of the known solutions to Eq. (8) for spatially inhomogeneous states¹⁴ correspond to the special case of Maxwell molecules, namely, a repulsive potential of the form $V(r) \sim r^{-4}$. For this potential, the collision rate $gI(g, \hat{\mathbf{k}})$ is independent of the relative velocity and this allows the infinite hierarchy of velocity moments to be recursively solved in some specific situations. Furthermore, the NS transport coefficients η_0 and κ_0 can be exactly obtained from the Chapman-Enskog method.² They are given by

$$\eta_0 = \frac{p}{\nu}, \quad \kappa_0 = \frac{15}{4} \frac{k_B}{m} \eta_0, \quad (15)$$

where $\nu = \theta n$, θ being an eigenvalue of the linearized Boltzmann collision operator.¹⁵

In this paper we are interested in studying the planar Couette flow for a dilute gas. We consider a gas enclosed between two parallel plates in relative motion and maintained at different temperatures. Under these conditions, the system is driven out of equilibrium by the combined action of the velocity and thermal gradients along the direction normal to the plates. After a transient period, the gas is expected to reach a steady state and the corresponding Boltzmann equation reads

$$v_y \frac{\partial}{\partial y} f = J[f, f], \quad (16)$$

where we have chosen the axis y as the one normal to the plates. In general, this equation must be solved subjected to specific boundary conditions. Nevertheless, in the same spirit as in the Chapman-Enskog method,² one may look for “normal” solutions in which all the space dependence of the distribution function occurs through a functional dependence on the hydrodynamic fields. The normal solution describes the state of the gas in the hydrodynamic regime, namely, for times much longer than the mean free time and for distances from the walls much larger than the mean free path. As mentioned in the Introduction, it has been proved^{3,4} that, in the case of Maxwell molecules, Eq. (16) admits an exact solution corresponding to the planar Couette flow problem. This solution belongs to the *normal* class, so that no explicit boundary conditions appear. In other words, all the space dependence of f is given through the local density, the local velocity, the local temperature, and their gradients. The solution is characterized by hydrodynamic profiles that are a simple generalization of those predicted by the NS approximation, Eqs. (5)–(7), namely

$$p = \text{const}, \quad (17)$$

$$\frac{1}{\nu(y)} \frac{\partial u_x}{\partial y} \equiv a = \text{const}, \quad (18)$$

$$\left[\frac{1}{\nu(y)} \frac{\partial}{\partial y} \right]^2 T = -\text{Pr} \frac{2m}{k_B} \gamma(a). \quad (19)$$

The dimensionless parameter $\gamma(a)$ is a nonlinear function of the reduced shear rate a that, by construction, behaves as $\gamma \approx a^2/5$ in the limit $a \rightarrow 0$. Again, the temperature can be seen as a quadratic function of the flow velocity, but now the coefficient η_0/κ_0 appearing in Eq. (7) is replaced by a shear-rate dependent coefficient $(\eta_0/\kappa_0)5\gamma(a)/a^2$. Furthermore, in this solution the pressure tensor is independent of the thermal gradient and the heat flux vector is linear in the thermal gradient, but all these fluxes are nonlinear functions of the shear rate. This nonlinear dependence can be characterized through five generalized transport coefficients. First, the shear stress P_{xy} defines a generalized shear viscosity $\eta(a)$ as

$$P_{xy} = -\eta(a) \frac{\partial u_x}{\partial y} \equiv -\eta_0 F_\eta(a) \frac{\partial u_x}{\partial y}. \quad (20)$$

Analogously, the component of the heat flux parallel to the thermal gradient defines a generalized thermal conductivity coefficient $\kappa_{yy}(a)$:

$$q_y = -\kappa_{yy}(a) \frac{\partial T}{\partial y} \equiv -\kappa_0 F_\kappa(a) \frac{\partial T}{\partial y}. \quad (21)$$

The dimensionless functions $F_\eta(a)$ and $F_\kappa(a)$ are the most relevant quantities of the problem. They are related to the function $\gamma(a)$ by $\gamma(a) = a^2 F_\eta(a)/5F_\kappa(a)$. Normal stress differences are different from zero and are measured by two viscometric functions $\Psi_{1,2}(a)$ defined by

$$\frac{P_{yy} - P_{xx}}{p} = \Psi_1(a)a^2, \quad (22)$$

$$\frac{P_{zz} - P_{yy}}{p} = \Psi_2(a)a^2. \quad (23)$$

Another interesting quantity related with the pressure tensor is the friction coefficient $\mu(a) = -P_{xy}/P_{yy}$. To NS order, we simply have $\mu(a) = a$. In the non-Newtonian regime, we generalize this coefficient as $\mu(a) = aF_\mu(a)$, where the friction function $F_\mu(a)$ is

$$F_\mu(a) = \frac{F_\eta(a)}{1 - [\Psi_2(a) - \Psi_1(a)]a^2/3}. \quad (24)$$

Finally, there exists a nonzero component of the heat flux orthogonal to the thermal gradient given by

$$q_x = -\kappa_{xy}(a) \frac{\partial}{\partial y} T \equiv -\kappa_0 \Phi(a) a \frac{\partial}{\partial y} T. \quad (25)$$

The three functions $\Psi_{1,2}(a)$ and $\Phi(a)$ are generalizations of Burnett coefficients. In fact, $\Psi_1(0) = -14/5$, $\Psi_2(0) = 4/5$, and $\Phi(0) = -7/2$ for Maxwell molecules and for hard spheres in the first Sonine approximation.² The determination of the nonlinear transport coefficients F_η , F_κ , $\Psi_{1,2}$, and Φ would imply the solution of an infinite hierarchy that cannot be solved in a recursive way.³ This hierarchy can only be solved step by step when one performs a perturbation expansion in powers of the shear rate. In fact, Tij and Santos⁴ determined the solution up to super-Burnett order:

$$F_\eta(a) = 1 - 3.111a^2 + \mathcal{O}(a^4), \quad (26)$$

$$F_\kappa(a) = 1 - 7.259a^2 + \mathcal{O}(a^4). \quad (27)$$

From Eqs. (26) and (27) it follows that $\gamma(a) = (a^2/5)[1 + 4.148a^2 + \mathcal{O}(a^4)]$. In addition, $F_\mu(a) = 1 - 1.911a^2 + \mathcal{O}(a^3)$.

Although the above analyses are valuable, they have two main limitations. On the one hand, they are restricted to the special case of Maxwell molecules. For other interaction potentials (e.g., hard spheres), the collisional moments involve all the moments of the distribution function and, as a consequence, the hydrodynamic profiles (17)–(19) are not *strictly* true. On the other hand, even for Maxwell molecules, the above perturbative solution is not useful for finite shear rates. These two limitations can be overcome, in the context of analytical methods, by introducing additional approximations, such as the Grad method,¹⁰ or by describing the system by means of kinetic models.^{5,7–9} In these approaches one explicitly gets the full nonlinear shear-rate dependence of the transport coefficients in a non-perturbative way. Moreover, the results are *universal*, namely the functions $F_\eta(a)$, $F_\kappa(a)$, ... are independent of the interaction potential, provided that the reduced shear rate is defined as in Eq. (18) with $\nu = p/\eta_0$.

The thirteen-moment Grad method consists of replacing the actual distribution by

$$f \rightarrow f_L \left\{ 1 + \frac{m}{n(k_B T)^2} \left[\left(\frac{mV^2}{5k_B T} - 1 \right) \mathbf{V} \cdot \mathbf{q} + \frac{1}{2} (P_{ij} - p\delta_{ij}) V_i V_j \right] \right\}, \quad (28)$$

where

$$f_L = n \left(\frac{m}{2\pi k_B T} \right)^{3/2} \exp \left(-\frac{mV^2}{2k_B T} \right) \quad (29)$$

is the local equilibrium distribution function. When the approximation (28) is inserted into the Boltzmann equation (8) and velocity moments are taken, one gets a closed set of equations for n , \mathbf{u} , \mathbf{P} , and \mathbf{q} . According to the geometry of the planar Couette flow, there are eight independent moments instead of the original thirteen moments appearing in Eq. (28). Risso and Cordero^{10,16} found that the set of independent moment equations, neglecting nonlinear terms

in the fluxes, admits a solution consistent with the profiles (17)–(19). In addition, they obtained explicit expressions for the transport coefficients introduced above as nonlinear functions of the reduced shear rate a . Those expressions are displayed in the Appendix.

Now we consider the kinetic model approach. The basic idea is to replace the detailed Boltzmann collision operator by a much simpler term that otherwise retains the main physical properties of the original operator $J[f, f]$. The most familiar choice is the BGK model,¹

$$J[f, f] \rightarrow -\nu(f - f_L), \quad (30)$$

where ν is an effective collision frequency that depends on the temperature, according to the interaction potential. The NS transport coefficients of the BGK model are $\eta_0 = p/\nu$ and $\kappa_0 = 5pk_B/2m\nu$. Thus the BGK model has the drawback that it predicts an incorrect value for the Prandtl number, $\text{Pr} = 1$. This is a consequence of the fact that ν is the only adjustable parameter in the model. This deficiency is corrected by the so-called ellipsoidal statistical (ES) model,¹ in which case

$$J[f, f] \rightarrow -\zeta(f - f_R), \quad (31)$$

where ζ is again an effective collision frequency and the reference function f_R is

$$f_R = n\pi^{-3/2}(\det \mathbf{A})^{-1/2} \exp(-\mathbf{A}^{-1} : \mathbf{VV}), \quad (32)$$

where $A_{ij} = (2k_B T/m)\text{Pr}^{-1}\delta_{ij} - 2(\text{Pr}^{-1} - 1)P_{ij}/mn$. The NS coefficients are now $\eta_0 = p/(\zeta\text{Pr}^{-1})$ and $\kappa_0 = 5pk_B/2m\zeta$. If, as in Eq. (15), we define a collision frequency $\nu = p/\eta_0$, then $\nu = \zeta\text{Pr}^{-1}$ in the ES model. Note that the ES model reduces to the BGK model if we formally make $\text{Pr} = 1$. Therefore, the ES model can be seen as an extension of the BGK model to account for the correct Prandtl number, which can be particularly relevant in the Couette flow where heat and momentum transport are coupled. The results derived from the BGK and the ES models for the Couette flow problem are also given in the Appendix. Apart from obtaining the transport properties, the velocity distribution function can be explicitly written. In particular, the BGK distribution is given by⁶

$$f(\mathbf{r}, \mathbf{v}) = n \left(\frac{m}{2\pi k_B T} \right)^{3/2} \frac{2\alpha(1+\alpha)^{3/2}}{\epsilon|\xi_y|} \int_{t_0}^{t_1} dt [2t - (1-\alpha)t^2]^{-5/2} \times \exp \left\{ -\frac{2\alpha}{1+\alpha} \frac{1-t}{\epsilon\xi_y} - \frac{1+\alpha}{2t - (1-\alpha)t^2} \left[\left(\xi_x + \frac{2a\alpha}{1+\alpha} \frac{1-t}{\epsilon} \right)^2 + \xi_y^2 + \xi_z^2 \right] \right\}. \quad (33)$$

Here, $(t_0, t_1) = (0, 1)$ if $\xi_y > 0$ and $(t_0, t_1) = [1, 2/(1-\alpha)]$ if $\xi_y < 0$. Besides, $\xi \equiv (m/2k_B T)^{1/2}\mathbf{V}$,

$$\alpha = \frac{\epsilon}{(\epsilon^2 + 8\gamma)^{1/2}}, \quad (34)$$

and

$$\epsilon = \left(\frac{2k_B T}{m} \right)^{1/2} \frac{1}{\nu} \frac{\partial}{\partial y} \ln T \quad (35)$$

is a (local) reduced thermal gradient. Equation (33) shows that the distribution function is a highly nonlinear function of the reduced gradients a and ϵ .

In Ref. 9 a comparison between the analytical results obtained from the Grad method and the BGK and ES models with those obtained from molecular dynamics simulations¹⁰ for hard disks was carried out. It was found that the three theories reproduced quite well the simulation data for F_η , but the Grad method failed for F_κ and Φ . The latter quantity was reproduced better by the ES model than by the BGK model. Notwithstanding this, more definite conclusions could not be reached because the simulation data were restricted to rather small shear rates, namely $a \lesssim 0.2$. In this range of shear rates, non-Newtonian effects are not especially significant. In addition, although the molecular dynamics simulations correspond to a very dilute gas (area fraction $\phi \approx 1\%$), the collisional contributions to the transport coefficients (absent in a Boltzmann description) are not *strictly* zero. Finally, as a minor point, conclusions drawn in the context of two-dimensional systems should not be extrapolated without caution to the more realistic case of three dimensions. As said in the Introduction, the aim of this paper is to solve numerically the Boltzmann equation by means of the DSMC method for the planar Couette flow and compare the results with the theoretical predictions. We will consider three-dimensional systems of Maxwell molecules and hard spheres subjected to shear rates as large as $a \simeq 1.2$. In addition to the nonlinear transport coefficients, the comparison will be extended to the level of the velocity distribution function itself.

III. BOUNDARY CONDITIONS AND MONTE CARLO SIMULATION

A. Boundary conditions

The goal now is to solve numerically the Boltzmann equation corresponding to the planar Couette flow by using the successful DSMC method.¹¹ The gas is enclosed between two parallel plates located at $y = 0$ and $y = L$, which are moving along the x -direction with velocities $\mathbf{U}_0 = U_0\hat{\mathbf{x}}$ and $\mathbf{U}_L = U_L\hat{\mathbf{x}}$, respectively. In addition, they are kept at temperatures T_0 and T_L , respectively. In order to solve Eq. (16), we need to impose the corresponding boundary conditions. They can be expressed in terms of the kernels $K_{0,L}(\mathbf{v}, \mathbf{v}')$ defined as follows. When a particle with velocity \mathbf{v}' hits the wall at $y = L$, the probability of being reemitted with a velocity \mathbf{v} within the range $d\mathbf{v}$ is $K_L(\mathbf{v}, \mathbf{v}')d\mathbf{v}$; the kernel $K_0(\mathbf{v}, \mathbf{v}')$ represents the same but at $y = 0$. The boundary conditions are then¹⁷

$$\Theta(\pm v_y)|v_y|f(y = \{0, L\}, \mathbf{v}) = \Theta(\pm v_y) \int d\mathbf{v}' |v_y'| K_{0,L}(\mathbf{v}, \mathbf{v}') \times \Theta(\mp v_y')f(y = \{0, L\}, \mathbf{v}', t). \quad (36)$$

In this paper we consider boundary conditions of complete accommodation with the walls, so that $K_{0,L}(\mathbf{v}, \mathbf{v}') = K_{0,L}(\mathbf{v})$ does not depend on the incoming velocity \mathbf{v}' and can be written as

$$K_{0,L}(\mathbf{v}) = A_{0,L}^{-1} \Theta(\pm v_y)|v_y| \phi_{0,L}(\mathbf{v}), \quad A_{0,L} = \int d\mathbf{v} \Theta(\pm v_y)|v_y| \phi_{0,L}(\mathbf{v}), \quad (37)$$

where $\phi_{0,L}(\mathbf{v})$ represents the probability distribution of a fictitious gas in contact with the system at $y = \{0, L\}$. Equation (37) can then be interpreted as meaning that when a particle hits a wall, it is absorbed and then replaced by a particle leaving the fictitious bath. Of course, any choice of $\phi_{0,L}(\mathbf{v})$ must be consistent with the imposed wall velocities and temperatures, i.e.,

$$U_{0,L} = \int d\mathbf{v} v_x \phi_{0,L}(\mathbf{v}), \quad (38)$$

$$k_B T_{0,L} = \frac{1}{3} m \int d\mathbf{v} (\mathbf{v} - \mathbf{U}_{0,L})^2 \phi_{0,L}(\mathbf{v}). \quad (39)$$

The simplest and most common choice is that of a Maxwell-Boltzmann (MB) distribution:

$$\phi_{0,L}^{\text{MB}}(\mathbf{v}) = \left(\frac{m}{2\pi k_B T_{0,L}} \right)^{3/2} \exp \left[-\frac{m(\mathbf{v} - \mathbf{U}_{0,L})^2}{2k_B T_{0,L}} \right]. \quad (40)$$

Under these conditions, the system is understood to be enclosed between two independent baths *at equilibrium*. While the conditions (40) are adequate for analyzing boundary effects,^{1,18} they are not very efficient when one is interested in obtaining the transport properties in the bulk region. In order to inhibit the influence of boundary effects, it is more convenient to imagine that the two fictitious baths are in *nonequilibrium* states resembling the state of the actual gas near the walls. More specifically, we can assume that the fictitious gases are described by the BGK equation, whose exact solution for the steady planar Couette flow is given by Eq. (33). In this case, the probability distributions $\phi_{0,L}(\mathbf{v})$ are

$$\begin{aligned} \phi_{0,L}^{\text{BGK}}(\mathbf{v}) = & \pi^{-3/2} \frac{m}{k_B T_{0,L}} \frac{\alpha_{0,L}(1 + \alpha_{0,L})^{3/2}}{\epsilon_{0,L}|v_y|} \int_{t_0}^{t_1} dt [2t - (1 - \alpha_{0,L})t^2]^{-5/2} \\ & \times \exp \left\{ -\left(\frac{2k_B T_{0,L}}{m} \right)^{1/2} \frac{2\alpha_{0,L}}{1 + \alpha_{0,L}} \frac{1 - t}{\epsilon_{0,L} v_y} - \frac{m}{2k_B T_{0,L}} \frac{1 + \alpha_{0,L}}{2t - (1 - \alpha_{0,L})t^2} \right. \\ & \left. \times \left[\left(v_x - U_{0,L} + \frac{2a\alpha_{0,L}}{1 + \alpha_{0,L}} \frac{1 - t}{\epsilon_{0,L}} \right)^2 + v_y^2 + v_z^2 \right] \right\}, \end{aligned} \quad (41)$$

where $(t_0, t_1) = (0, 1)$ if $v_y > 0$ and $(t_0, t_1) = [1, 2/(1 - \alpha_{0,L})]$ if $v_y < 0$, and $\alpha_{0,L} = \epsilon_{0,L}/[\epsilon_{0,L}^2 + 8\gamma_{\text{BGK}}(a')]^{1/2}$. Here, a' is the *estimated* value of the reduced shear rate, as predicted by the BGK model for specific values of the boundary parameters $U_{0,L}$ and $T_{0,L}$, and $\gamma_{\text{BGK}}(a')$ is obtained from Eq. (A6). Given the values of the four independent boundary

parameters $U_{0,L}$ and $T_{0,L}$ (as well as the distance L), the shear rate a' and the local thermal gradients $\epsilon_{0,L}$ are fixed by the conditions (17)–(19). Therefore,

$$a' = \frac{U_L - U_0}{\mathcal{L}}, \quad (42)$$

$$\epsilon_{0,L} = \frac{1}{\mathcal{L}} \left(\frac{2k_B T_{0,L}}{m} \right)^{1/2} \left[\frac{T_L - T_0}{T_{0,L}} \pm \frac{m\gamma_{\text{BGK}}(a')\text{Pr}}{k_B T_{0,L}} \mathcal{L}^2 \right]. \quad (43)$$

In these equations, \mathcal{L} is related to the actual separation L between the plates through the nonlinear equation

$$L = \int_0^{\mathcal{L}} \frac{ds}{\nu(s)}, \quad (44)$$

where s is a variable in terms of which the temperature is a quadratic function, namely $T(s) = T_0[1 + \epsilon_0(m/2k_B T_0)^{1/2}s - m\gamma_{\text{BGK}}(a')\text{Pr}s^2/k_B T_0]$, and the s -dependence of the collision frequency $\nu(s)$ appears only through the temperature (taking into account that $p = \text{const}$). The solution of the nonlinear set of equations (42)–(44) gives a' , $\epsilon_{0,L}$, and \mathcal{L} for any choice of $U_{0,L}$, $T_{0,L}$, and L . Nevertheless, from a practical point of view, it is more convenient to fix U_0 , $T_{0,L}$, a' , and ϵ_0 as independent parameters. Without loss of generality we take $U_0 = 0$ and $T_L = 1$. In addition, we will choose $\epsilon_0 = 0$. This implies that, if boundary effects were absent, the temperature would have a maximum at the lower plate $y = 0$. Thus,

$$U_L = a'\mathcal{L}, \quad \mathcal{L} = \left[\frac{\Delta}{2\text{Pr}\gamma_{\text{BGK}}(a')} \right]^{1/2}, \quad (45)$$

$$\epsilon_L = -2\frac{\Delta}{\mathcal{L}}. \quad (46)$$

In the above equations $\Delta \equiv T_0 - 1$ and we have taken $m = 1$ and $k_B = \frac{1}{2}$. Finally, the actual distance L is given by Eq. (44). However, from the simulation point of view, it is more useful to express L in terms of the collision frequency $\bar{\nu}$ corresponding to the temperature T_L and the average density \bar{n} . In other words, instead of Eq. (44) we use

$$\bar{n} = \frac{1}{L} \int_0^L dy n(y) = \frac{1}{L} \int_0^{\mathcal{L}} ds \frac{n(s)}{\nu(s)} \quad (47)$$

to determine L . For the sake of concreteness, let us consider repulsive potentials, for which $\nu = \bar{\nu}(n/\bar{n})(T/T_L)^\omega$, where ω ranges from 0 (Maxwell molecules) to $\frac{1}{2}$ (hard spheres). In that case,

$$L = \frac{1}{\bar{\nu}} \int_0^{\mathcal{L}} ds [T(s)]^{-\omega}. \quad (48)$$

For Maxwell molecules, this simply reduces to $L = \mathcal{L}/\bar{\nu}$, while for hard spheres one has $L = (\mathcal{L}/\bar{\nu}) \tan^{-1}(\sqrt{\Delta})/\sqrt{\Delta}$. In summary, given the values of a' and Δ , the separation L between the plates and the velocity of the upper plate U_L are uniquely determined. In addition, the thermal gradient at the upper plate ϵ_L is also determined, while the value at the lower plate is fixed as $\epsilon_0 = 0$. The knowledge of these boundary parameters allows one to obtain the distributions $\phi_{0,L}^{\text{BGK}}(\mathbf{v})$, according to Eq. (41).

B. The DSMC method

Now, we briefly describe the numerical algorithm we have employed to solve the Boltzmann equation by means of the so-called Direct Simulation Monte Carlo (DSMC) method.¹¹ In this method, the velocity distribution function is represented by the velocities $\{\mathbf{v}_i\}$ and positions $\{y_i\}$ of a sufficiently large number of particles N . Given the geometry of the problem, the physical system is split into layers of width δy , sufficiently smaller than the mean free path. The velocities and coordinates are updated from time t to time $t + \delta t$, where the time step δt is much smaller than the mean free time, by applying a streaming step followed by a collision step. In the *streaming step*, the particles are moved ballistically, $y_i \rightarrow y_i + v_{iy}\delta t$. In addition, those particles crossing the boundaries are reentered with velocities sampled

from the corresponding probability distribution $K_{0,L}(\mathbf{v})$. Suppose that a particle i crosses the lower plate between times t and $t + \delta t$, i.e., $y_i + v_{iy}\delta t < 0$. Then, regardless of the incoming velocity \mathbf{v}_i , a new velocity $\tilde{\mathbf{v}}_i$ is assigned according to the following rules. First, a velocity $\tilde{\mathbf{v}}_i$ (with $\tilde{v}_{iy} > 0$) is sampled with a probability proportional to $|v_y|\phi_0^{\text{MB}}(\mathbf{v})$. If one is considering the MB boundary conditions, this velocity is accepted directly. Otherwise, the above acts as a “filter” to optimize the acceptance-rejection procedure and the velocity $\tilde{\mathbf{v}}_i$ is accepted with a probability proportional to the ratio $\phi_0^{\text{BGK}}(\mathbf{v})/\phi_0^{\text{MB}}(\mathbf{v})$. If the velocity is rejected, a new velocity $\tilde{\mathbf{v}}_i$ is sampled and the process is repeated until acceptance. The new position is assigned as $\tilde{v}_{iy}(\delta t + y_i/v_{iy})$. The process is analogous in the case of the upper plate.

The *collision step* proceeds as follows. For each layer α , a pair of potential collision partners i and j are chosen at random with equiprobability. The collision between those particles is then accepted with a probability equal to the corresponding collision rate times δt . For hard spheres, the collision rate is proportional to the relative velocity $|\mathbf{v}_i - \mathbf{v}_j|$, while it is independent of the relative velocity for Maxwell molecules (an angle cut-off is needed in the latter case). If the collision is accepted, the scattering direction is randomly chosen according to the interaction law and post-collisional velocities are assigned to both particles, according to the conservation of momentum and energy. After the collision is processed or if the pair is rejected, the routine moves again to the choice of a new pair until the required number of candidate pairs has been processed.

In the course of the simulations, the following “coarse-grained” local quantities are computed. The number density in layer α is

$$n_\alpha = \bar{n} \frac{N_\alpha}{(N/L)\Delta y} = \frac{\bar{n}L}{N\Delta y} \sum_{i=1}^N \Theta_\alpha(y_i), \quad (49)$$

where $\Theta_\alpha(y)$ is the characteristic function of layer α , i.e., $\Theta_\alpha(y) = 1$ if y belongs to layer α and is zero otherwise. Similarly, the flow velocity, the temperature, the pressure tensor, and the heat flux of layer α are

$$\mathbf{u}_\alpha = \frac{1}{N_\alpha} \sum_{i=1}^N \Theta_\alpha(y_i) \mathbf{v}_i, \quad (50)$$

$$k_B T_\alpha = \frac{p_\alpha}{n_\alpha} = \frac{m}{3N_\alpha} \sum_{i=1}^N \Theta_\alpha(y_i) (\mathbf{v}_i - \mathbf{u}_\alpha)^2, \quad (51)$$

$$\mathbf{P}_\alpha = \frac{L}{N\Delta y} m \sum_{i=1}^N \Theta_\alpha(y_i) (\mathbf{v}_i - \mathbf{u}_\alpha)(\mathbf{v}_i - \mathbf{u}_\alpha), \quad (52)$$

$$\mathbf{q}_\alpha = \frac{L}{N\Delta y} \frac{m}{2} \sum_{i=1}^N \Theta_\alpha(y_i) (\mathbf{v}_i - \mathbf{u}_\alpha)^2 (\mathbf{v}_i - \mathbf{u}_\alpha). \quad (53)$$

From these quantities one can get local values of the gradients and of the transport coefficients. For instance, the reduced shear rate is

$$a_\alpha = \frac{\bar{n}}{\nu n_\alpha} \left(\frac{T_L}{T_\alpha} \right)^\omega \frac{u_{\alpha+1,x} - u_{\alpha,x}}{\delta y} \quad (54)$$

and the viscosity function is

$$F_{\eta,\alpha} = -\frac{P_{\alpha,xy}}{a_\alpha p_\alpha}. \quad (55)$$

As said before, in the simulations we take units such that $m = 1$, $T_L = 1$, and $k_B = \frac{1}{2}$. It remains to fix the time unit or, equivalently, the length unit. The standard definition of mean free path in the case of hard spheres is²

$$\lambda = \frac{1}{\sqrt{2}n\pi\sigma^2}, \quad (56)$$

where σ is the diameter of the spheres. The Navier-Stokes shear viscosity is (in the first Sonine approximation) $\eta_0 = 5(mk_B T/\pi)^{1/2}/16\sigma^2$. Consequently, the effective collision frequency $\nu = p/\eta_0$ and the mean free path λ are related as $\nu = (8/5\sqrt{\pi})(2k_B T/m)^{1/2}/\lambda$. As usual, we choose the mean free path corresponding to the average density \bar{n} as the length unit. This in turn implies that $\bar{\nu} = 8/5\sqrt{\pi} \simeq 0.903$. For convenience, we take the latter value for Maxwell molecules as well. The typical values of the simulation parameters are $N = 2 \times 10^5$ particles, a layer width $\delta y = 0.02$, and a time step $\delta t = 0.003$.

The procedure to measure the relevant quantities of the problem is as follows. First the values of the imposed shear rate a' and the temperature difference Δ are chosen. This choice fixes the system size L , as well as the upper velocity U_L and the upper thermal gradient ϵ_L , according to Eqs. (45), (46), and (48). Starting from an equilibrium initial state with $T = T_0$, the system evolves driven by the boundary conditions described before. After a transient period (typically up to $t = 25$), the system reaches a steady state in which the quantities fluctuate around constant values. In this state, the balance equations predict that the quantities u_y , P_{xy} , P_{yy} , and $u_x P_{xy} + q_y$ are spatially uniform and this is used in the simulations as a test to make sure that the steady state has been achieved. Once the steady state is reached, the local quantities (49)–(55) are averaged over typically 100 snapshots equally spaced between $t = 25$ and $t = 55$.

C. Test of the numerical algorithm

Before closing this Section, it is worthwhile carrying out a test of the reliability of the numerical method. To that end, we have simulated the BGK equation by a DSMC-like method similar to the one described in Ref. 19. If the boundary conditions are implemented correctly and the simulation parameters are well chosen, then the simulation results should agree with the theoretical BGK predictions. We have checked that this indeed the case. As an example, consider the hard-sphere situation with $a' = 1$ and $\Delta = 5$. This corresponds to $\gamma_{\text{BGK}} = 0.248$, $L = 1.81$, $U_L = 3.17$, and $\epsilon_L = -3.15$, where in this case $\text{Pr} = 1$. Figure 1 shows the marginal velocity distributions of particles reemitted by the walls,

$$\mathcal{K}_{0,L}(\xi_y) = \left(\frac{2k_B T_{0,L}}{m} \right)^{1/2} \int_{-\infty}^{\infty} dv_x \int_{-\infty}^{\infty} dv_z K_{0,L}(\mathbf{v}), \quad (57)$$

as functions of $\xi_y = (m/2k_B T_{0,L})^{1/2} v_y$. The case $\xi_y > 0$ ($\xi_y < 0$) corresponds to particles that are reemitted from the lower (upper) plate. The agreement with the imposed distribution is excellent. Note the strong asymmetry between the distributions corresponding to both plates, in contrast to the symmetry of the MB distributions obtained from (40). The temperature and velocity profiles are shown in Fig. 2. The simulation values overlap, within statistical fluctuations, with the theoretical predictions. Apart from the profiles, we have verified that the generalized transport coefficients obtained from the fluxes also agree with the theory. A more stringent test is provided in Fig. 3, where the marginal distribution function

$$\varphi(\xi_y) = \frac{1}{n} \left(\frac{2k_B T}{m} \right)^{1/2} \int_{-\infty}^{\infty} dv_x \int_{-\infty}^{\infty} dv_z f(\mathbf{v}), \quad \xi_y = \left(\frac{m}{2k_B T} \right)^{1/2} v_y \quad (58)$$

is plotted at the point $y/L = 0.5$, which corresponds to a local thermal gradient $\epsilon = -0.60$. It is apparent again that an excellent agreement exists between simulation and theory.

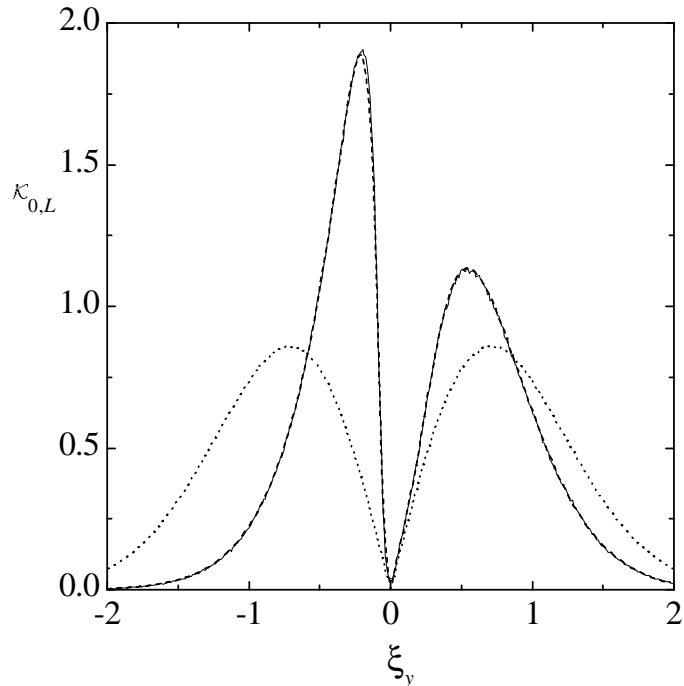


FIG. 1. Plot of the marginal distribution function of particles reemitted by the walls. The solid line corresponds to the distribution measured in the simulation by applying the BGK boundary conditions (with $a' = 1$, $\epsilon_0 = 0$, and $\epsilon_L = -3.15$), the dashed line is the theoretical BGK distribution (which is hardly distinguishable from the solid line), and the dotted line corresponds to the MB boundary conditions.

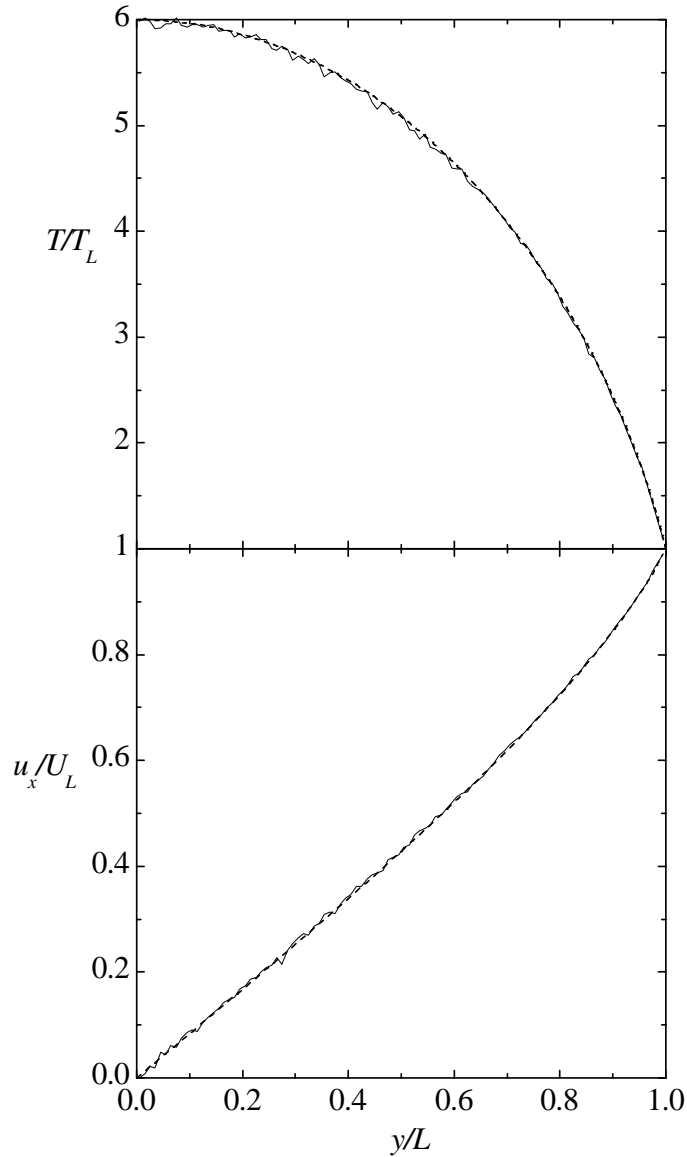


FIG. 2. Temperature and velocity profiles for hard spheres in the case $L = 1.81$, $U_L = 3.17$, and $T_L = 6$. The solid lines are results obtained from a DSMC simulation of the BGK equation, while the dashed lines are the theoretical BGK results.

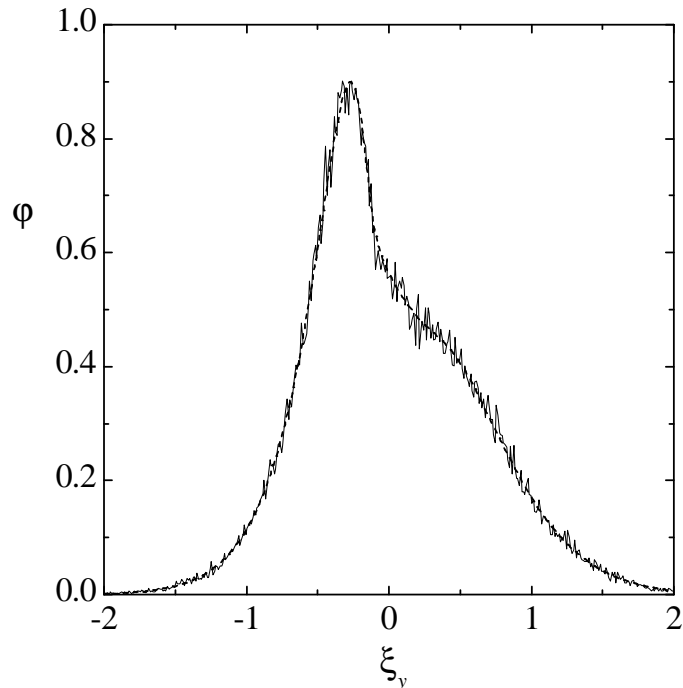


FIG. 3. Marginal velocity distribution function for hard spheres at $y = 0.5L$ in the case $L = 1.81$, $U_L = 3.17$, and $T_L = 6$. The solid line is obtained from a DSMC simulation of the BGK equation, while the dashed line (which is hardly distinguishable from the solid line) is the theoretical BGK distribution.

IV. RESULTS

This Section is devoted to a comparison between the simulation results for the Boltzmann equation obtained by the simulation method described in the previous Section and the theoretical predictions provided by the Grad method and the BGK and ES kinetic models. The comparison will be carried out at the levels of the transport coefficients and the velocity distribution, both for Maxwell molecules and hard spheres. Before that, the hydrodynamic profiles obtained from the simulations by using the two types of boundary conditions considered to in Sec. III are presented.

A. Hydrodynamic profiles

As said in Secs. I and II, the Boltzmann equation for Maxwell molecules admits an exact solution characterized by Eqs. (17)–(19). This solution applies to the bulk region, i.e., the region where boundary effects are negligible. Obviously, in a simulation with a finite size of the system, it is not possible to avoid boundary effects completely. On the other hand, one can expect that the “nonequilibrium” boundary conditions based on the BGK distribution, Eq. (41), inhibit the boundary effects, as compared with the conventional “equilibrium” boundary conditions (40). We have confirmed that this is indeed the case. As an illustrative example, let us consider $\Delta = 5$ and $a' = 0.92$ for Maxwell molecules. This corresponds to $\gamma_{\text{BGK}} = 0.21$, $L = 4.68$, $U_L = 3.90$, and $\epsilon_L = -2.37$. Figure 4 shows the temperature and velocity profiles as obtained by using the MB and BGK boundary conditions. It is apparent that the velocity slips and the temperature jumps at the walls are much larger in the former case than in the latter. Note that the maximum temperature is not exactly located in the layer adjacent to the lower plate but it is slightly shifted. It is interesting to remark that when plotting the temperature T as a function of the flow velocity u_x , a parabolic curve is observed with both boundary conditions, as expected from Eqs. (18) and (19). A more evident proof of the advantage of the BGK conditions is shown in Fig. 5. Since the pressure is a constant in the exact solution valid in the bulk, any deviation from $p = \text{const}$ can be attributed to boundary effects. The pressure obtained with the BGK boundary conditions is practically constant, except near the upper plate, while the one obtained with the MB conditions is only nearly constant in a small region around $y/L \simeq 0.75$. Finally, Fig. 6 shows the ratio a/a' between the actual (local) shear rate a measured in the simulations, cf. Eq. (54), and the imposed shear rate a' . The ratio is closer to 1 in the case of the BGK boundary conditions than in that of the MB conditions. In addition, in the former case the region where a is practically constant extends to layers closer to the lower plate.

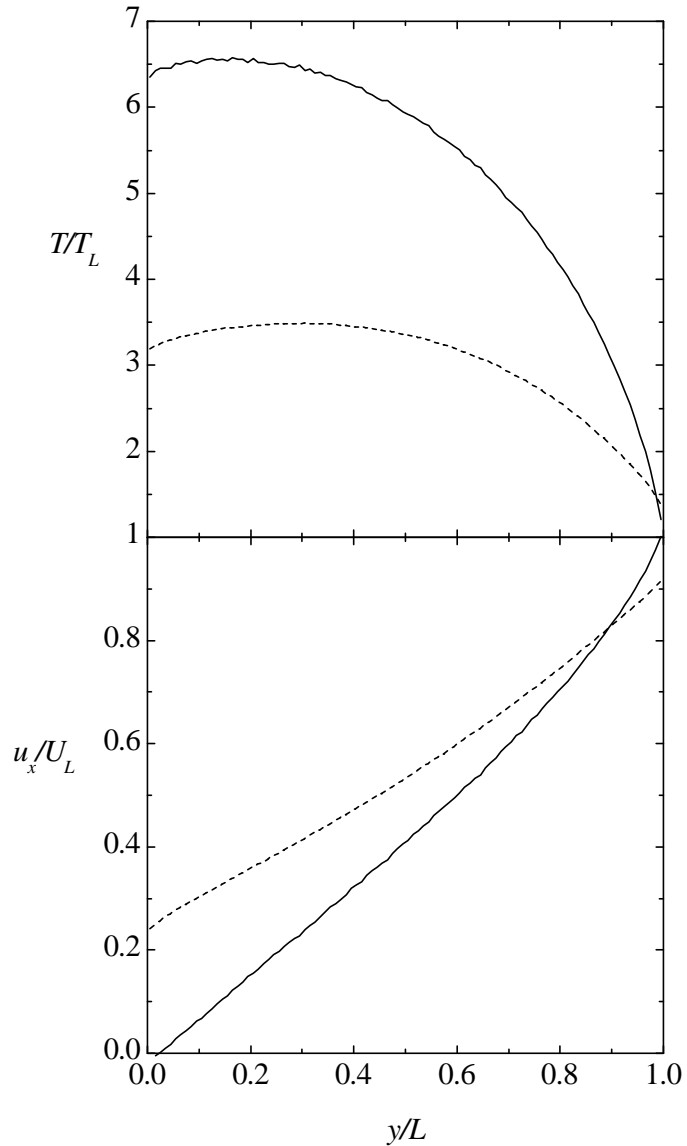


FIG. 4. Temperature and velocity profiles for Maxwell molecules, as obtained from DSMC simulations, in the case $L = 4.68$, $U_L = 3.90$, and $T_L = 6$. The solid lines refer to the results obtained from the BGK boundary conditions and the dashed lines refer to those obtained from the MB boundary conditions.

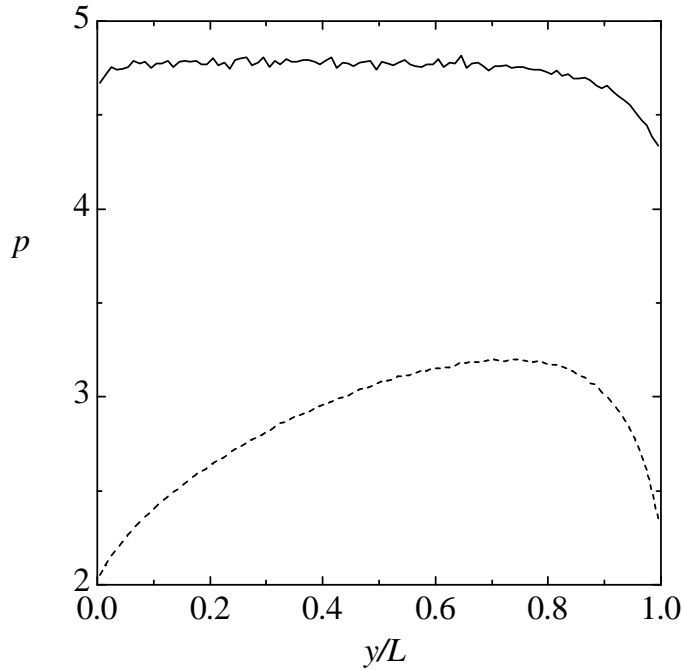


FIG. 5. Same as in Fig. 4, but for the pressure (which is measured in units of $\bar{n}k_B T_L$).

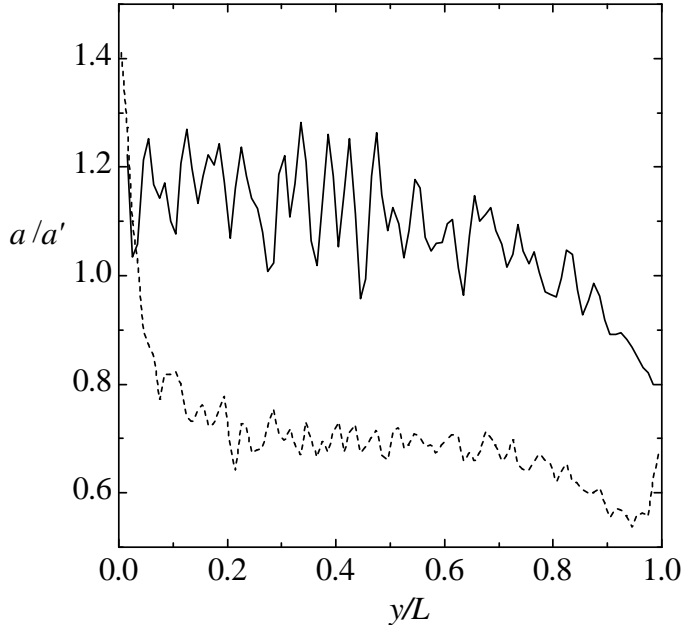


FIG. 6. Same as in Fig. 4, but for the ratio a/a' between the actual shear rate, a , and the one imposed by the BGK boundary conditions, a' .

In summary, the above example illustrates that the BGK boundary conditions are much more efficient than the MB ones to measure transport properties in the bulk. Therefore, in what follows we will only consider the BGK conditions. In each case, we identify a bulk domain comprised between the layers $y = y_0$ and $y = y_1$ where $a \simeq \text{const}$, $p \simeq \text{const}$, and $\gamma \simeq \text{const}$, and take averages of a , F_η , F_κ , $\Psi_{1,2}$, and Φ over those layers. Typical values are $y_0/L \simeq 0.2$ and $y_1/L \simeq 0.8$.

B. Nonlinear transport coefficients

In this subsection we compare the simulation results for Maxwell molecules and hard spheres obtained from the Monte Carlo simulations with the (universal) predictions of the Grad method and the BGK and ES kinetic models.

An interesting quantity in the *nonlinear* Couette flow is the parameter γ , which is related to the curvature of the temperature profile. Its shear-rate dependence is shown in Fig. 7. A remarkable feature is that the simulation data for both interactions seem to lie on a common curve. This indicates that, as predicted by the models, the transport properties are hardly sensitive to the interaction potential, provided that the quantities are conveniently scaled. While the kinetic models exhibit a good quantitative (in the case of the ES model) or qualitative (BGK model) agreement, the Grad method fails, except for small shear rates. Since $\gamma(a) = a^2 F_\eta(a)/5F_\kappa(a)$, one can interpret $5\gamma(a)/a^2$ as an effective, shear-rate dependent Prandtl number (relative to the usual Pr). This quantity is bounded between 1 for small shear rates and $5/3$ (in the BGK model) or $5/2$ (in the ES model) in the limit of large shear rates. This is consistent with the fact that the BGK model underestimates the value of γ .

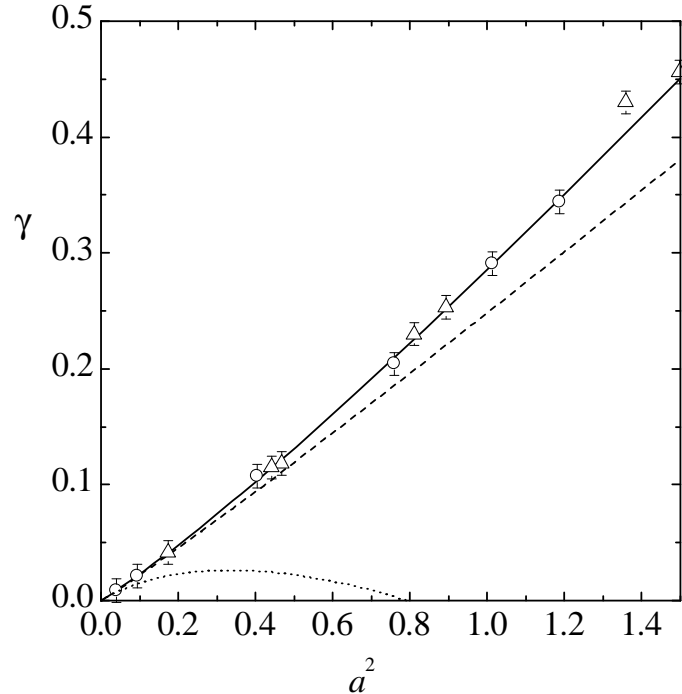


FIG. 7. Plot of the thermal curvature parameter γ as a function of the shear rate. The symbols are simulation data for Maxwell molecules (circles) and for hard spheres (triangles), while the lines are the theoretical predictions given by the ES kinetic model (solid line), the BGK kinetic model (dashed line), and the Grad method (dotted line).

The most important transport coefficient is the nonlinear viscosity represented by the function $F_\eta(a)$. According to Fig. 8, the three theories retain the qualitative trends of the simulation data, namely the decrease of F_η with increasing a (shear thinning effect). In general, however, the kinetic models (especially the BGK model) have a better agreement than the Grad method. It is also interesting to remark that a slight influence of the interaction potential seems to exist, the shear thinning effect being a little bit more significant for hard spheres than for Maxwell molecules. The nonlinear thermal conductivity $F_\kappa(a)$ is plotted in Fig. 9. It is quite apparent that Grad's solution does not capture even the qualitative shape of F_κ , as was already noted in the case of hard disks.⁹ Again, the kinetic models present a good agreement, especially in the case of the ES model.

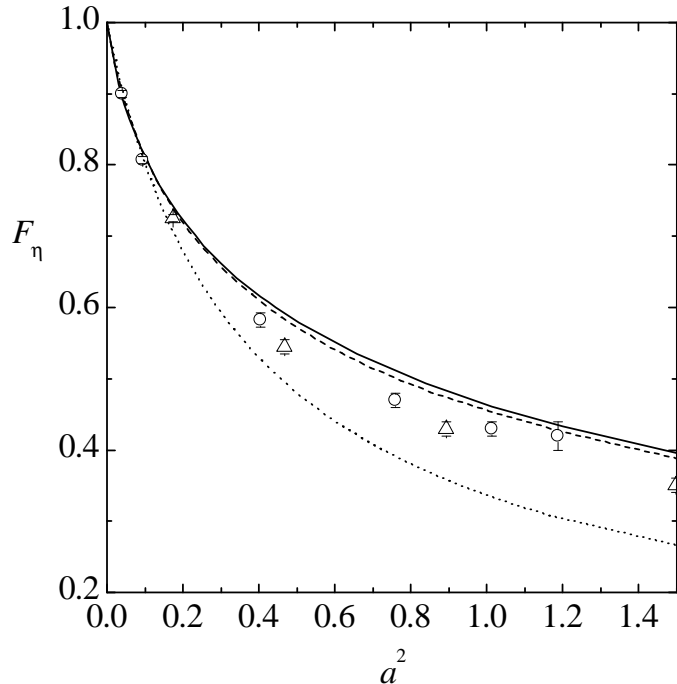


FIG. 8. Same as in Fig. 7, but for the viscosity function F_η .

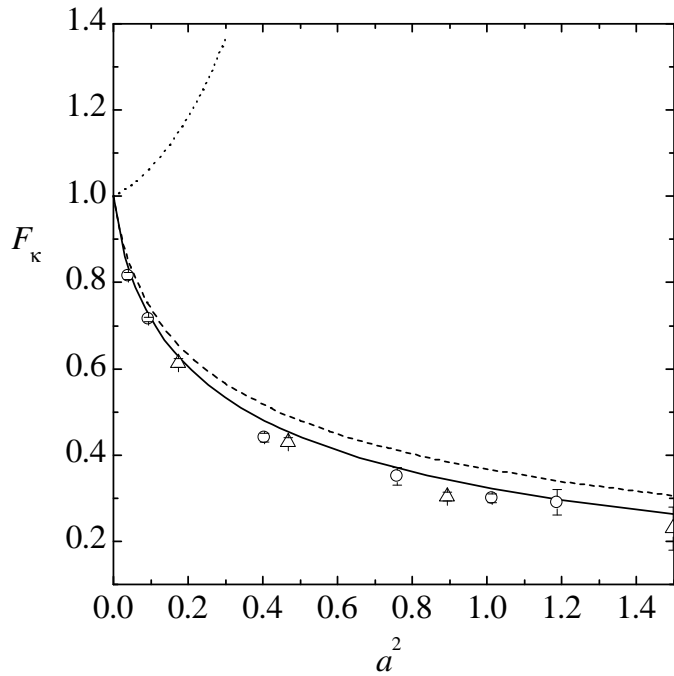


FIG. 9. Same as in Fig. 7, but for the thermal conductivity function F_κ .

Normal stress differences are characterized by the viscometric functions $\Psi_{1,2}(a)$. These quantities are well described by the kinetic models, as shown in Figs. 10 and 11. At a quantitative level, the agreement is better in the case of Maxwell molecules. In fact, the viscometric functions, especially the second one, exhibit a certain influence of the potential. The functions $\Psi_{1,2}(a)$ were not evaluated from the Grad method in Refs. 10 and 16. On the other hand, the friction function $F_\mu(a)$ was calculated from the Grad method.^{10,16} This quantity is plotted in Fig. 12, showing an agreement between the theories and the simulation data similar to the one found in Fig. 8 for the viscosity function. The last transport coefficient is the cross-coefficient Φ defined by Eq. (25). The comparison with simulation results for this quantity is a stringent test of the theories, since it is a generalization of a Burnett coefficient, measuring the component of the heat flux orthogonal to the thermal gradient and induced by the shearing. Figure 13 shows that, as

happened with the thermal conductivity function $F_\kappa(a)$, the Grad method gives a wrong prediction for the shear-rate dependence of $\Phi(a)$. On the other hand, the kinetic models describe fairly well the nonlinear behavior of this function, especially in the case of the ES model.

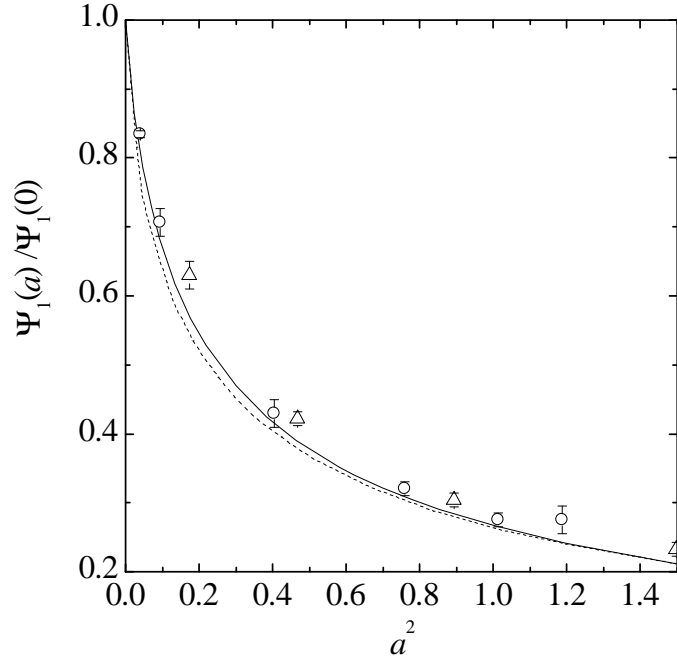


FIG. 10. Same as in Fig. 7, but for the first viscometric function Ψ_1 , relative to the Burnett value $\Psi_1(0)$. Note that the Grad prediction is not plotted.

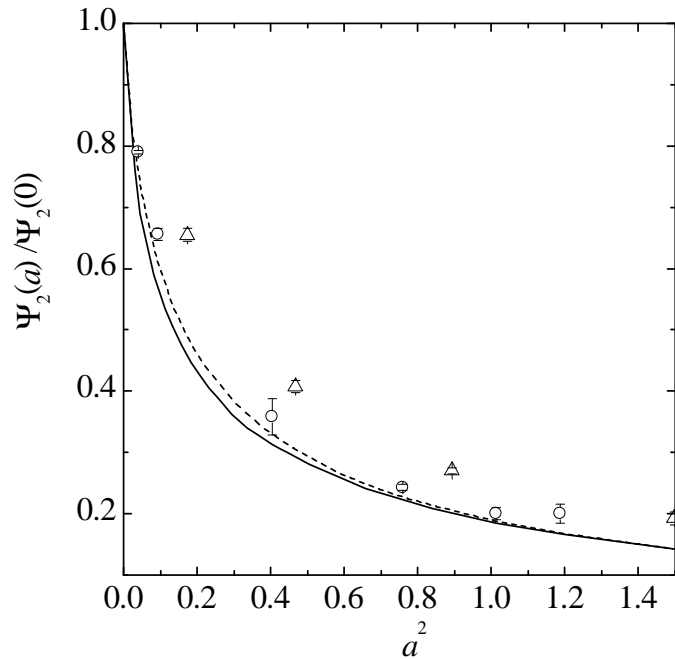


FIG. 11. Same as in Fig. 7, but for the second viscometric function Ψ_2 , relative to the Burnett value $\Psi_2(0)$. Note that the Grad prediction is not plotted.

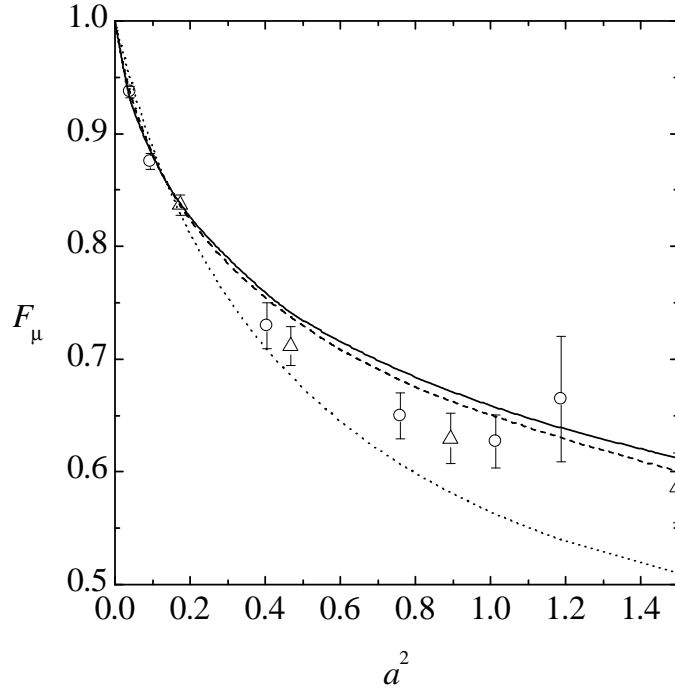


FIG. 12. Same as in Fig. 7, but for the friction function F_μ .

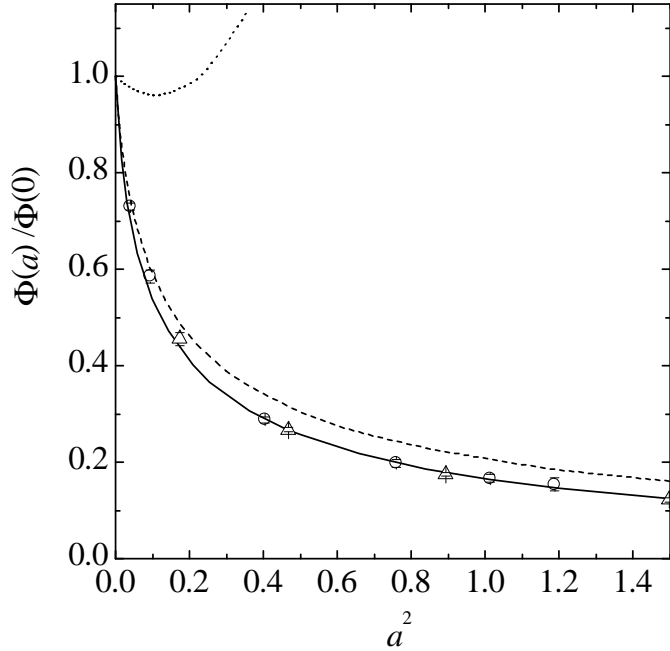


FIG. 13. Same as in Fig. 7, but for the cross coefficient Φ , relative to the Burnett value $\Phi(0)$.

C. Velocity distribution function

Apart from the transport coefficients, the kinetic models provide the velocity distribution function. In the case of the BGK model, the solution is given by Eq. (33), while the ES distribution function can be found in Refs. 8 and 9. In order to assess their reliability, we have computed in the simulations the marginal distribution (58) at the layer $y/L = 0.5$. The ratio $R(\xi_y) \equiv \varphi(\xi_y)/[\pi^{-1/2} \exp(-\xi_y^2)]$ is a measure of the departure of the distribution function from the local equilibrium. This quantity is plotted in Fig. 14 for Maxwell molecules in the case of a reduced shear rate $a = 0.636$ and a reduced (local) thermal gradient $\epsilon = -0.272$. Both theories capture the main features of the actual distribution. While the BGK distribution exhibits a better agreement near the maximum (around $\xi_y \simeq -0.5$), the ES distribution seems to describe better the region $\xi_y \gtrsim 1$. The case of hard spheres is illustrated in Fig. 15, which

corresponds to $a = 0.419$ and $\epsilon = -0.195$. In this case, the ES model shows a superiority over the BGK model both near the maximum and for large positive velocities.

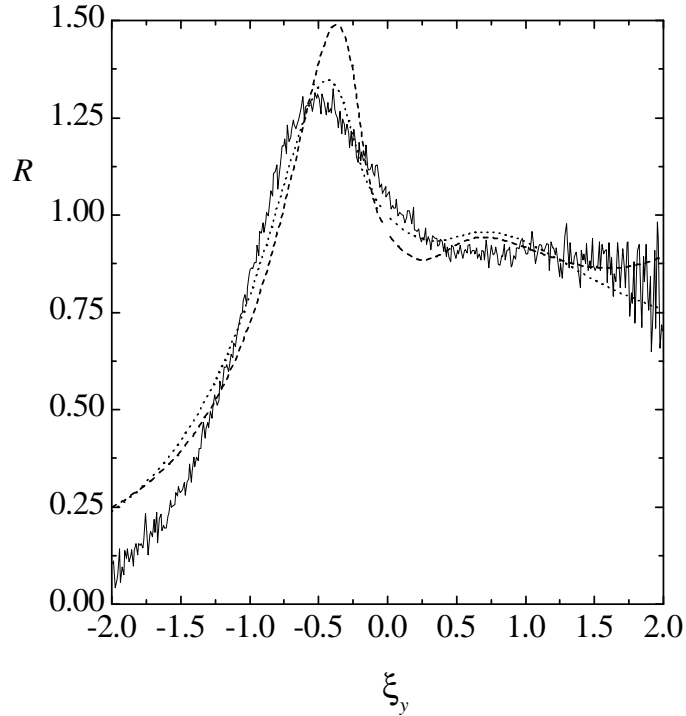


FIG. 14. Marginal velocity distribution function, relative to the local equilibrium distribution, for Maxwell molecules at $y = 0.5L$ in the case $a = 0.636$ and $\epsilon = -0.272$. The solid line is obtained from a DSMC simulation, while the dashed line is the theoretical ES distribution and the dotted line is the theoretical BGK distribution.

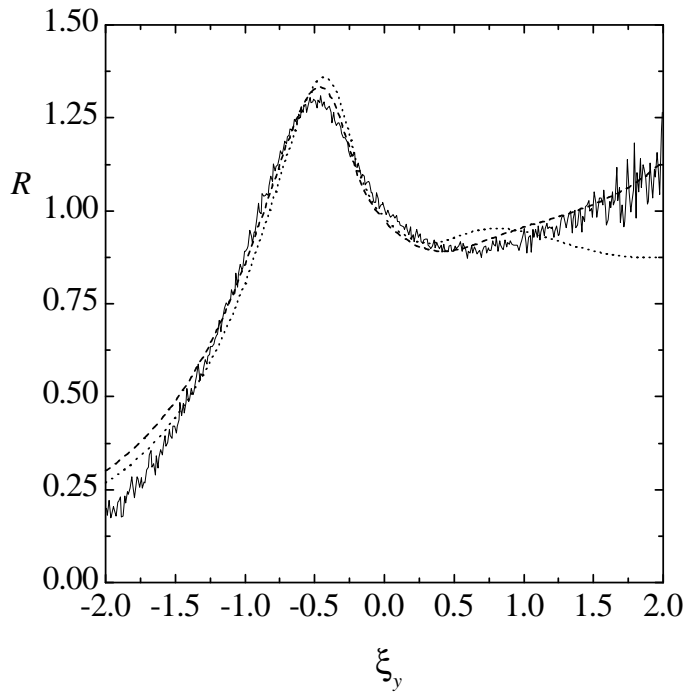


FIG. 15. Same as in Fig. 13, but for hard spheres in the case $a = 0.419$ and $\epsilon = -0.195$.

V. CONCLUDING REMARKS

This paper has dealt with the steady planar Couette flow in a dilute gas beyond the scope of the Navier-Stokes description. This nonlinear problem had been previously studied by means of kinetic theory tools, such as the Grad method, and the BGK and ES kinetic models. These theories predict momentum and heat fluxes characterized by five shear-rate dependent generalized transport coefficients: a viscosity function $F_\eta(a)$, Eq. (20), a thermal conductivity function $F_\kappa(a)$, Eq. (21), two viscometric functions $\Psi_{1,2}(a)$, Eqs. (22) and (23), and a cross coefficient $\Phi(a)$, Eq. (25). The main motivation of our study has been to perform DSMC simulations for Maxwell molecules and hard spheres in order to assess the reliability of the above theories in the non-Newtonian regime. Since we have been interested in the bulk properties, we have used “nonequilibrium” boundary conditions to inhibit the influence of finite-size effects.

An important outcome of the simulation results is that, as predicted by the kinetic theories considered here, the shear-rate dependence of the transport coefficients is practically insensitive to the interaction potential when the quantities are properly nondimensionalized. In particular, the actual shear rate has been reduced with respect to an effective collision frequency defined from the Navier-Stokes shear viscosity coefficient. The simulation results show, however, that the second viscometric function presents a non negligible influence of the interaction model, so that the normal stress difference $P_{zz} - P_{yy}$ is smaller for Maxwell molecules than for hard spheres. The comparison with the theoretical predictions shows that the kinetic models give a fairly good description of the five transport coefficients. On the other hand, the Grad method yields a shear viscosity in qualitative agreement with the simulations but it dramatically fails for the coefficients measuring the heat flux. This is basically due to the truncation scheme of the Grad method at the level of the heat flux. The physical idea behind a kinetic model is quite different, since it consists of replacing the true Boltzmann collision operator by a simple relaxation term but otherwise all the velocity moments are taken into account. As a consequence, while in the Grad method one has to solve a closed set of coupled differential equations for the moments, in the case of the kinetic model one gets the velocity distribution function and determines the fluxes from it.

In the ES kinetic model the reference distribution function appearing in the collision operator is an anisotropic Gaussian parameterized by the pressure tensor. This allows the model to give the correct Prandtl number $\text{Pr} = \frac{2}{3}$ but at the expense of complicating its mathematical structure. In the case of the BGK model, however, the reference distribution is that of local equilibrium but the model leads to $\text{Pr} = 1$. The agreement with simulation of the ES model is generally better than that of the BGK model, especially in the case of F_κ and Φ . In spite of this, it is fair to say that the performance of the BGK model is quite good, given its simplicity relative to that of the ES model. Finally, the results reported in this paper clearly shows the usefulness of kinetic models to analyze nonlinear transport phenomena in the Couette flow problem. This complements previous conclusions drawn from other nonlinear problems, such as the uniform shear flow and the Fourier flow.

APPENDIX: THEORETICAL EXPRESSIONS FOR THE TRANSPORT COEFFICIENTS

In this Appendix we list the explicit shear-rate dependence of the dimensionless transport coefficients defined in Sec. II, according to the Grad method, the BGK model, and the ES model.

1. The Grad method

From the Appendix of Ref. 10, corrected in Ref. 16, one has

$$F_\eta(a) = \frac{2}{1 + \frac{72}{25}a^2 + \Delta(a)}, \quad (\text{A1})$$

$$F_\kappa(a) = \frac{4}{1 - \frac{216}{25}a^2 + 3\Delta(a)}, \quad (\text{A2})$$

$$\Phi(a) = -7 \frac{1 - \frac{36}{125}a^2}{1 + \frac{6}{5}a^2 + (1 - \frac{63}{25}a^2)\Delta(a)}, \quad (\text{A3})$$

where $\Delta(a) \equiv \sqrt{1 + \frac{116}{25}a^2 - \frac{864}{625}a^4}$. The viscometric functions are not evaluated in Refs. 10 and 16, although the friction function is provided. It is given by

$$F_\mu(a) = \frac{2}{1 + \frac{12}{25}a^2 + \Delta(a)}. \quad (\text{A4})$$

Note that $F_\eta(a)$ and $F_\mu(a)$ become meaningless for $a^2 \geq 25(\sqrt{1057} + 29)/432 \simeq 3.56$, while $F_\kappa(a)$ and $\Phi(a)$ are unphysical for $a^2 \geq 50/63 \simeq 0.79$. For small shear rates, the above transport coefficients behave as $F_\eta \simeq 1 - \frac{13}{5}a^2$, $F_\kappa \simeq 1 + \frac{21}{50}a^2$, $\Phi \simeq -\frac{7}{2}(1 - \frac{197}{250}a^2)$, and $F_\mu \simeq 1 - \frac{7}{5}a^2$.

2. The BGK model

The derivation of the transport coefficients from the BGK model⁵ implies the resummation of asymptotic series by means of the Borel method. As a consequence, the results are expressed in terms of the functions $F_r(x)$ defined by the recurrence relation $F_r(x) = [(d/dx)x]^r F_0(x)$, where

$$F_0(x) = \frac{2}{x} \int_0^\infty dt t e^{-t^2/2} K_0(2t^{1/2}/x^{1/4}), \quad (\text{A5})$$

K_0 being the zeroth-order modified Bessel function. The curvature parameter $\gamma(a)$ is given by the solution to the following implicit equation

$$a^2 = \gamma \frac{3F_1 + 2F_2}{F_1}, \quad (\text{A6})$$

where the functions F_r are evaluated at $x = \gamma$. Next, the transport coefficients are expressed in terms of a and $F_r(\gamma)$ as

$$F_\eta(a) = F_0, \quad (\text{A7})$$

$$F_\kappa(a) = \frac{F_0}{5} \frac{3F_1 + 2F_2}{F_1}, \quad (\text{A8})$$

$$\Psi_1(a) = -2F_1 \frac{3F_1 + 4F_2}{3F_1 + 2F_2}, \quad (\text{A9})$$

$$\Psi_2(a) = 4 \frac{F_1 F_2}{3F_1 + 2F_2}, \quad (\text{A10})$$

$$\Phi(a) = -[5F_2 + 2F_3 + a^2(F_2 + 5F_3 + 8F_4 + 4F_5)]. \quad (\text{A11})$$

For small shear rates, one gets $F_\eta \simeq 1 - \frac{18}{5}a^2$, $F_\kappa \simeq 1 - \frac{162}{25}a^2$, $\Psi_1 \simeq -\frac{14}{5}(1 - \frac{1476}{175}a^2)$, $\Psi_2 \simeq \frac{4}{5}(1 - \frac{288}{25}a^2)$, $\Phi \simeq -\frac{14}{5}$, and $F_\mu \simeq 1 - \frac{12}{5}a^2$.

3. The ES model

In Refs. 8 and 9 the solution of the ES model is worked out keeping the Prandtl number Pr as a free parameter. Here we particularize the results to the correct value $\text{Pr} = \frac{2}{3}$. It is convenient to express the transport coefficients in terms of an auxiliary parameter β , defined as the solution of the implicit equation

$$a^2 = \frac{4\beta}{9} \frac{[2\beta(F_1 + 2F_2) - 3]^2 [3F_1 + 2F_2 - 2\beta F_1(F_1 + 2F_2)]}{F_0^2 [2\beta(F_1 + F_2) - 3] + F_1 [2\beta(F_1 + 2F_2) - 3]^2}, \quad (\text{A12})$$

where now the functions F_r are evaluated at $x = \beta$. The relationship between the curvature parameter γ and β is

$$\gamma(a) = \frac{2}{9} \beta [3 - 2\beta(F_1 + 2F_2)]. \quad (\text{A13})$$

The transport coefficients are

$$F_\eta(a) = \frac{9F_0}{[2\beta(F_1 + 2F_2) - 3]^2}, \quad (\text{A14})$$

$$F_\kappa(a) = \frac{a^2}{5\gamma(a)} F_\eta(a), \quad (\text{A15})$$

$$\Psi_1(a) = -\frac{12\beta}{a^2} \frac{3F_1 + 4F_2 - 2\beta F_1(F_1 + 2F_2)}{(3 - 2\beta F_1)[3 - 2\beta F_1(F_1 + 2F_2)]}, \quad (\text{A16})$$

$$\Psi_2(a) = \frac{24\beta}{a^2} \frac{F_2}{(3 - 2\beta F_1)[3 - 2\beta F_1(F_1 + 2F_2)]}, \quad (\text{A17})$$

$$\begin{aligned} \Phi(a) = & \frac{1}{40} C_1 \{ a^2 [C_1^4 F_0^3 (F_1 + 2F_2) - 9C_1^3 F_0^2 (F_2 + 2F_3) + 54C_1^2 F_0 (F_2 + 4(F_3 + F_4)) \\ & - 108C_1 (F_2 + 5F_3 + 4(2F_4 + F_5))] - C_3 (C_1 F_0 F_1 - 6F_2) + 4C_1^2 F_0 (F_1 + 2F_2) \\ & + 4C_1 [C_2 F_0 F_1 - 6(F_2 + 2F_3)] - 24C_2 F_2 \}. \end{aligned} \quad (\text{A18})$$

In Eq. (A18),

$$C_1 \equiv \frac{3}{3 - 2\beta(F_1 + 2F_2)}, \quad (\text{A19})$$

$$C_2 \equiv \frac{3}{3 - 2\beta F_1}, \quad (\text{A20})$$

$$C_3 \equiv 3a^2 C_1^3 F_0^2 + 4C_2 \{2\beta[C_1(F_1 + 4F_2) + 3F_1] - 3C_1\}. \quad (\text{A21})$$

For small shear rates, one has $F_\eta \simeq 1 - \frac{21}{5}a^2$, $F_\kappa \simeq 1 - \frac{197}{25}a^2$, $\Psi_1 \simeq -\frac{14}{5}(1 - \frac{2126}{175}a^2)$, $\Psi_2 \simeq \frac{4}{5}(1 - \frac{413}{25}a^2)$, $\Phi \simeq -\frac{7}{2}$, and $F_\mu \simeq 1 - 3a^2$.

^{a)} Electronic mail: jmm@unex.es

^{b)} Electronic mail: andres@unex.es

^{c)} Electronic mail: vicenteg@unex.es

¹ C. Cercignani, *Mathematical Methods in Kinetic Theory* (Plenum Press, New York, 1990).

² S. Chapman and T. G. Cowling, *The Mathematical Theory of Nonuniform Gases* (Cambridge University Press, Cambridge, 1970).

³ N. K. Makashev and V. I. Nosik, “Steady-state Couette flow (with heat transfer) of a gas of Maxwellian molecules,” Dokl. Akad. Nauk SSSR **253**, 1077 (1980) [Sov. Phys. Dokl. **25**, 589 (1981)]; V. I. Nosik, “Degeneration of the Chapman-Enskog expansion in one-dimensional motions of Maxwellian molecule gases,” in *Rarefied Gas Dynamics 13*, edited by O. M. Belotserkovskii, M. N. Kogan, S. S. Kutateladze, and A. K. Rebrov (Plenum Press, New York, 1983), Vol. 1, pp. 237–244.

⁴ M. Tij and A. Santos, “Combined heat and momentum transport in a dilute gas,” Phys. Fluids **7**, 2858 (1995).

⁵ J. J. Brey, A. Santos, and J. W. Dufty, “Heat and momentum transport far from equilibrium,” Phys. Rev. A **36**, 2842 (1987).

⁶ C. S. Kim, J. W. Dufty, A. Santos, and J. J. Brey, “Analysis of nonlinear transport in Couette flow,” Phys. Rev. A **40**, 7165 (1989).

⁷ V. Garzó and M. López de Haro, “Kinetic model for heat and momentum transport,” Phys. Fluids **6**, 3787 (1994).

⁸ V. Garzó and M. López de Haro, “Nonlinear transport for a dilute gas in steady Couette flow,” Phys. Fluids **9**, 776 (1997).

⁹ J. M. Montanero and V. Garzó, “Nonlinear Couette flow in a dilute gas: Comparison between theory and molecular-dynamics simulation,” Phys. Rev. E **58**, 1836 (1998).

¹⁰ D. Risso and P. Cordero, “Dilute gas Couette flow: Theory and molecular-dynamics simulation,” *Phys. Rev. E* **56**, 489 (1997).

¹¹ G. A. Bird, *Molecular Gas Dynamics and the Direct Simulation of Gas Flows* (Clarendon, Oxford, 1994).

¹² R. Tehver, F. Toigo, J. Koplik, and J. R. Banavar, “Thermal walls in computer simulations,” *Phys. Rev. E* **57**, R17 (1998).

¹³ J. M. Montanero, M. Alaoui, A. Santos, and V. Garzó, “Monte Carlo simulation of the Boltzmann equation for steady Fourier flow,” *Phys. Rev. E* **49**, 367 (1994).

¹⁴ A. Santos and V. Garzó, “Exact non-linear transport from the Boltzmann equation,” in *Rarefied Gas Dynamics 19*, edited by J. Harvey and G. Lord (Oxford University Press, Oxford, 1995), Vol. 1, pp. 13–22.

¹⁵ J. A. McLennan, *Introduction to Nonequilibrium Statistical Mechanics* (Prentice-Hall, Englewood Cliffs, NJ, 1989).

¹⁶ D. Risso and P. Cordero, “Erratum: Dilute gas Couette flow: Theory and molecular-dynamics simulation [Phys. Rev. E **56**, 489 (1997)],” *Phys. Rev. E* **57**, 7365 (1998).

¹⁷ J. R. Dorfman and H. van Beijeren, “The kinetic theory of gases,” in *Statistical Mechanics*, Part B, edited by B. J. Berne (Plenum, New York), pp. 65–179.

¹⁸ D. C. Wadsworth, “Slip effects in a confined rarefied gas: I: Temperature slip,” *Phys. Fluids A* **5**, 1831 (1993).

¹⁹ J. M. Montanero, A. Santos, M. Lee, J. W. Dufty, and J. F. Lutsko, “Stability of uniform shear flow,” *Phys. Rev. E* **57**, 546 (1998).